Preprints, 3rd IFAC Workshop on Linear Parameter-Varying Systems
November 4-6, 2019. Eindhoven, The Netherlands

Data-Driven LPV Reference Tracking for a Control Moment Gyroscope ⋆

Tom Bloemers * **Roland Tóth** * **Tom Oomen** **

* *Control Systems Group, Department of Electrical Engineering, Eindhoven University of Technology, 5612 AE Eindhoven, The Netherlands (e-mail: {t.a.h.bloemers, r.toth}@tue.nl)*
** *Control Systems Technology, Department of Mechanical Engineering, Eindhoven University of Technology, 5612 AE Eindhoven, The Netherlands (e-mail: t.a.e.oomen@tue.nl).*

Abstract: A fixed order discrete-time linear parameter-varying (LPV) controller is designed directly from local frequency domain measurement data of a control moment gyroscope (CMG) with the goal to enable reference tracking over a wide operating range. Through a global parametrization of the LPV controller, local stability and performance guarantees can be posed on the system through frequency domain shaping methods. The capabilities of the proposed methodology are demonstrated on a simulation example of a CMG.

Keywords: Data-Driven Control, LPV Frequency Response Methods, Control Moment Gyroscope.

1. INTRODUCTION

Control moment gyroscopes (CMGs) are typically used e.g., to control the attitude of spacecrafts (Bedrossian et al., 2009; Kristiansen et al., 2005) or to provide roll stabilization for ships (Perez and Steinmann, 2009). A CMG consists of a rotating disk that is mounted in a gimbal assembly, where each of these gimbals can be rotated around their axis of rotation. Angular momentum is generated by the rotational velocity of the disk. Changing the angular position of the gimbals causes a re-direction of the angular momentum of the disk. This change in angular momentum causes a gyroscopic torque that reacts on the body to which the gimbals are mounted, resulting in e.g., a change of attitude of a spacecraft (Wie, 2008). CMGs exhibit nonlinear dynamics typically characterized by highly coupled behavior and challenging rotational dynamics, for which control design is a challenge. These setups are, therefore, often used as a benchmark for nonlinear control.

Control of CMGs has been widely studied. In (Liceaga et al., 2005) a multivariable linear time-invariant (LTI) controller has been designed, however the achievable range of operation was quite restricted due to the linearization. In (Reyhanoglu and van de Loo, 2006), this limitation was overcome through the design of a cascaded backstepping approach to develop state feedback controllers for reference tracking, however performance specifications are difficult to incorporate into such a design. The framework of linear parameter-varying (LPV) systems has been utilized in (Abbas et al., 2014; Theis et al., 2014; Koelewijn et al., 2018) to provide a systematic procedure to nonlinear CMG controller design for which performance specifications can be incorporated through frequency domain shaping.

In the literature, a lot of control designs have been tested on CMGs and it has been shown that the LPV framework provides efficient, model-based tools to design nonlinear controllers that enable a wide operating range. However, for many mechatronic systems, e.g., wafer scanners electromagnetic positioning devices or motor drives, it is difficult or not possible at all to derive high fidelity models that include flexible and position-dependent dynamics (Wassink et al., 2005). Therefore, a common practice in the industry is to derive controllers directly from frequency response function (FRF) measurements, opening possibilities for automated alternatives to classical controller tuning approaches (Maciejowski, 1989).

Although the framework of LPV systems has proven to be an effective tool to design controllers for nonlinear systems, at present these tools are at their infancy when a parametric model is not available. First steps towards data-driven controller design in the frequency domain have been made in (Kunze et al., 2007), where a gain-scheduled controller is synthesized through a characterization of local performance requirements in terms of lower bounds on the bandwidth and both gain and phase margins. In (Karimi and Emedi, 2013) a gain-scheduled controller is designed by imposing constraints in the Nyquist diagram, requiring the manual design of an open-loop transfer function in order to guarantee local stability and performance. On the other hand, a time-domain approach is presented in (Formentin et al., 2016), where a controller is identified such that the closed-loop will mimic an ideal behavior described in terms of a model-matching filter.

Inspired by these methods, the main contribution of this paper is to demonstrate how a discrete-time LPV controller can be directly obtained from local frequency

⋆ This work has received funding from the European Research Council (ERC) under the European Union's Horizon 2020 research and innovation programme (grant agreement nr. 714663).

domain measurement data of a CMG. The proposed methodology can be seen as an improved version of Kunze et al. (2007), in the sense that we formulate the desired control objectives in terms of a model-matching problem, which allows performance specifications to be incorporated in the design through frequency domain shaping filters. Through an a priori chosen discrete-time controller parametrization, a controller is obtained through convex optimization, for which local stability and performance is guaranteed. The capabilities of the synthesized controller are demonstrated through a simulation example on a CMG.

The paper is organized as follows: in Section 2, a description of the control moment gyroscope is given and the experiments to obtain frequency domain data about its behavior are discussed. Section 3 introduces the controller structure and an approach to the design of a data-driven LPV controller is discussed. This is followed by Section 4, where the capabilities of the LPV controller resulting from the data-driven design are demonstrated. Finally, conclusions are drawn in Section 5.

Notation: $\mathbb{R}$ denotes the set of real numbers. The notation x_j is used to indicate the j^{th} component of a vector $x \in \mathbb{R}^{n_x}$. We denote the imaginary unit by $i = \sqrt{-1}$ and $\Re\{\cdot\}$ and $\Im\{\cdot\}$ represent the real and imaginary parts of a complex variable, respectively. The set of all real rational proper and stable transfer functions is denoted by $\mathcal{RH}_\infty$.

2. GYROSCOPE

2.1 Plant description

A schematic overview of a CMG, with 3 gimbals, is presented in Figure 1. The gyroscope is comprised of a disk D, mounted in a gimbal assembly consisting of three gimbals A, B and C. The disk D, rotating with velocity $\dot{q}_1$, is contained in gimbal C. An input torque τ_2 is available to control the angle q_2 of gimbal C. This gimbal is in turn contained in gimbal B, which is assumed to be fixed in place ($q_3 \equiv 0$, as depicted in Figure 1) and contained in gimbal A. The angle q_4 of gimbal A can be thought of as, e.g., the orientation of a spacecraft, which we would like to control through input τ_2.

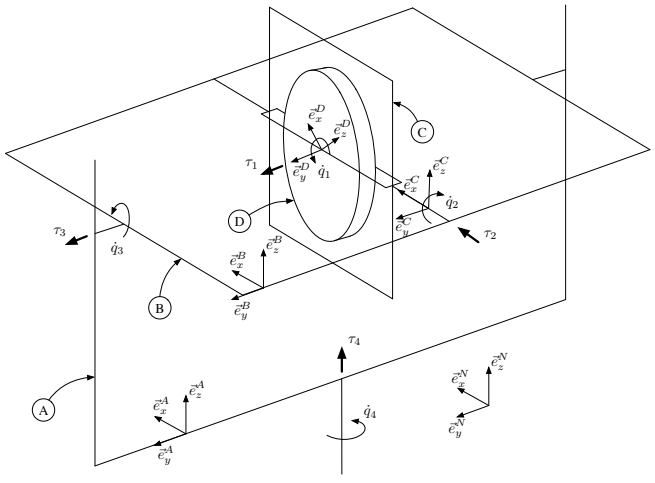

Fig. 1. Schematic overview of the 3-DOF gyroscope.

2.2 Dynamics

The gyroscope consists of three gimbals (A, B and C) along with a symmetric disk (D) as shown in Figure 1. Sets of right orientated orthogonal unit vectors e_i^j with $i = x, y, z$ and $j = A, B, C, D, N$ are attached to the bodies (A, B, C and D) and the natural (i.e., world) reference frame N respectively. The origins of the coordinate frames are located in the center of the disk D. Only rotational dynamics are considered as there are no translational dynamics. Furthermore, gravity effects can be neglected as it is assumed that the gyroscope is symmetric.

The equations of motion in the generalized coordinates q can be derived using the Euler-Lagrange equations, which results in a set of nonlinear equations of the form

$$F : \{\, \mathcal{M}(q(t))\ddot{q}(t) + \mathcal{C}(q(t), \dot{q}(t))\dot{q}(t) = \mathcal{J}(q)\tau, \tag{1}$$

where $q = [q_1\ q_2\ q_3\ q_4]^\top$ are the angular positions, $\tau = [\tau_1\ \tau_2\ \tau_3\ \tau_4]^\top$ are the input torques, $\mathcal{M}(q)$ is the inertia matrix, $\mathcal{C}(q, \dot{q})$ is the Coriolis matrix and $\mathcal{J}(q)$ selects input τ_2. Because of the complexity of the equations (1) they are not expressed in this paper, but they can be found in (Bloemers and Tóth, 2019).

The nonlinear model (1) is linearized around a moving equilibrium using a first-order Taylor series expansion at the operating points

$$\begin{aligned} q_* &\in [-\pi\ \ \pi]^4, \qquad \dot{q}_* = [\dot{q}_{1,*}\ 0\ 0\ 0]^\top, \\ \ddot{q}_* &= [0\ 0\ 0\ 0]^\top, \quad \tau_* = [0\ 0\ 0\ 0]^\top, \end{aligned} \tag{2}$$

with $\dot{q}_{1,*} \in [30\ 60]$. Note that $\dot{q}_{1,*} \neq 0$, hence a trajectory of $\dot{q}_{1,*}(t)$ in time defines an equilibrium family of (q_*, τ_*) in terms of (1). Furthermore, we assume that gimbal B is fixed and thus the dynamics describing the motion of gimbal B do not play any role. Additionally, it is assumed that the disk is controlled around an operating point and therefore, the dynamics of the disk are also neglected. For a given value of $\dot{q}_{1,*}$ this results in the linearized equations of motion

$$\mathcal{I}\dot{x}(t) = A(q_*, \dot{q}_*)x(t) + Bu(t) \tag{3a}$$

$$y(t) = q_4(t) \tag{3b}$$

where $x = [q_4\ \dot{q}_2\ \dot{q}_4]^\top : \mathbb{R} \to \mathbb{X} \subseteq \mathbb{R}^{n_x}$ is considered as the state variable, $u = \tau_2 : \mathbb{R} \to \mathbb{U} \subseteq \mathbb{R}^{n_u}$, $y = q_4 : \mathbb{R} \to \mathbb{Y} \subseteq \mathbb{R}^{n_y}$ are the input and output signals of (3a), respectively, and

$$\mathcal{I} = \begin{bmatrix} 1 & 0 & 0 \\ 0 & \mathcal{I}_1 & 0 \\ 0 & 0 & \mathcal{I}_2 \end{bmatrix}, \quad A(q_*, \dot{q}_*) = \begin{bmatrix} 1 & 0 & 0 \\ 0 & -f_C & J_D\dot{q}_{1,*} \\ 0 & -J_D\dot{q}_{1,*} & -f_A \end{bmatrix} \tag{4}$$

and $B = [0\ 1\ 0]^\top$ characterize the dynamic relations with $\mathcal{I}_1 = (I_C + I_D)$ and $\mathcal{I}_2 = (I_D + K_A + K_B + K_C)$. Here I_C, I_D, J_D, K_A, K_B and K_C are the scalar moments of inertia around the i^{th} $(i = x, y, z)$ axis, respectively, for the bodies A, B, C and D, while f_A and f_C are the viscous friction coefficients for bodies A and C, respectively. The numerical values of these parameters are given in Table 1. For a comparison of the linearized model (3a) versus the nonlinear model (1), see (Abbas et al., 2014).

2.3 Data-driven model

By observing (4), it is obvious that q_* and τ_* satisfying (2) do not influence the local dynamics, only $\dot{q}_{1,*}$ plays a role.

Table 1. Moments of inertia and viscous friction parameters for the gyroscope.

I_C	I_D	J_D	K_A
0.0010	0.0028	0.0056	0.0376
K_B	K_C	f_A	f_C
0.0213	0.0027	0.0080	0.0001

Hence, under the given assumptions, the linearization and the equilibrium points are characterized directly by only $\dot{q}_{1,*}$. As a consequence, an LPV form of (3a) is obtained by introducing the velocity of the disk as a so-called scheduling variable $p = w_c\dot{q}_{1,*} + m_c$, with $p \in \mathbb{P} = [-1, 1]$ and $\dot{q}_{1,*} \in [30, 60]$ (rad/s). Here w_c and m_c are used for normalization and centering, respectively. Furthermore, we assume that the system is sampled and actuated under a zero-order hold setting with a sampling rate $T_s = 0.005$ (s). FRF data of (3a), shown in Figure 2, is obtained at the set of frozen operating points $\{p^{(\tau)}\}_{\tau=1}^{N_p} = \mathcal{P} \subset \mathbb{P}$ corresponding to various disk speeds, given by an equidistant regular grid $\mathcal{P}$ that consists of $N_p = 11$ points; and a frequency grid $\{\omega^{(k)}\}_{k=1}^{N_\omega} = \Omega$ that consists of $N_\omega = 1000$ logarithmically spaced points in the frequency range $\Omega \subset [0, \pi]$. We denote these linear local models by $G_p(e^{i\omega})$, where p denotes the dependency on the scheduling variable. From the FRF data (Figure 2) it can be observed that the variation caused by a change in the velocity of the disk $\dot{q}_1$ reflects a change in the gain and a shift of resonance frequency.

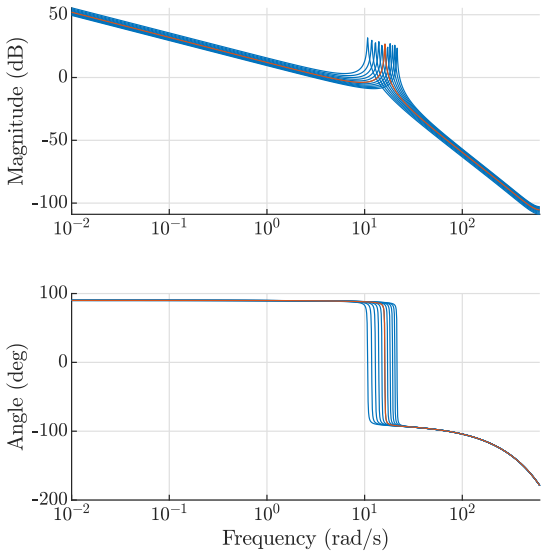

Fig. 2. Magnitude and phase plots of the FRF data of the gyroscope obtained at the operating points $\{p^{(\tau)}\}_{\tau=1}^{N_p} \subset [-1, 1]$ (rad/s) are plotted in blue and the nominal FRF at $p = 0$ (corresponding to $\dot{q}_{1,*} = 45$ (rad/s)) is plotted in orange.

3. DATA-DRIVEN LPV CONTROLLER SYNTHESIS

3.1 Objectives of control design

Controller design for the gyroscope (1) is considered in terms of the discrete-time closed-loop interconnection shown in Figure 3. Performance specifications for

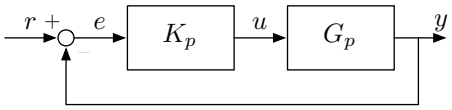

Fig. 3. Local LPV representation of the closed-loop interconnection. G_p is a linear system corresponding to the local behavior of F at the operating point p and K_p is an LPV controller scheduled by p.

this closed-loop system are expressed through a model-matching filter $M \in \mathcal{RH}_\infty$. The objective is to design a controller, scheduled by the p, such that (a) for all operating conditions, the local closed-loop system is stable and (b) for all operating conditions, the error between the set of closed-loop systems and the ideal closed-loop behavior expressed in terms of a model-matching filter is below an acceptable threshold. In other words, the goal is to design a controller K_p scheduled by p such that

(a) the local closed-loop transfer function in Figure 3

$$T_p(e^{i\omega}) = \frac{L_p(e^{i\omega})}{1 + L_p(e^{i\omega})}, \tag{5}$$

with $L_p(e^{i\omega}) = G_p(e^{i\omega})K_p(e^{i\omega})$, satisfies that $|\lambda(T_p(e^{i\omega}))| < 1\ \forall p \in \mathbb{P}$ with λ denoting the poles of a transfer function;

(b) the minimum of γ for which

$$\sup_{\omega\in\Omega} |T_p(e^{i\omega}) - M(e^{i\omega})| < \gamma,\ \forall p \in \mathbb{P} \tag{6}$$

is below an acceptable threshold $\gamma \geq 0$.

Condition (a) describes the local stability expectation, while (b) expresses the performance objective. The resulting controller K_p, dependent on p, can be thought of as a data-driven gain-scheduling based controller design, after which the controller can can be implemented as illustrated in Figure 4. In the remainder of this section, a solution is proposed to synthesize data-driven LPV controllers with respect to sampled data structures $\mathcal{P}$ and Ω.

3.2 Controller parametrization

We consider a fixed n_b-order FIR controller with following structure

$$K_p(e^{i\omega}) = \sum_{\ell=0}^{n_b} b_\ell(p)e^{-i\omega\ell} \tag{7}$$

where $b_\ell(p)$ is parametrized through a priori chosen set of basis functions

$$b_\ell(p) = \sum_{j=1}^{n} c_j^\ell \phi_j^\ell(p). \tag{8}$$

The basis functions $\{\phi_j\}_{j=1}^n$ can be chosen as rational, polynomial, affine or piecewise linear basis functions

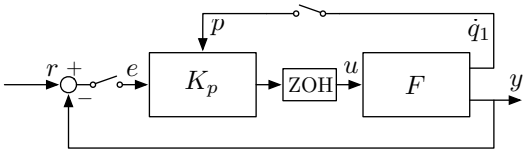

Fig. 4. Interpretation of the closed-loop implementation of the LPV controller with the plant. Here K_p is the discrete-time LPV controller scheduled by a time-varying p and F represents the continuous-time nonlinear system (1) where p is measured.

defining the function class to which the scheduling dependence of the controller is restricted to. The controller coefficients are collected in $\theta = \begin{bmatrix} c_1^0 & \dots & c_1^{n_b} & \dots & c_n^0 & \dots & c_n^{n_b} \end{bmatrix}$. An FIR controller structure is chosen for technical reasons, which will become apparent later on.

3.3 Performance characterization

The closed-loop performance expectations, with respect to requirement (b), are defined in terms of an ideal filter $M(e^{i\omega})$. A weighted $\mathcal{H}_\infty$ model-matching problem is considered in order to measure the performance objective with respect to the desired behavior $M(e^{i\omega})$

$$\begin{aligned} \min_{\theta} \quad & \gamma \\ \text{s.t.} \quad & |W(e^{i\omega}) \left(T_p(e^{i\omega}, \theta) - M(e^{i\omega})\right)| < \gamma \\ & \forall \omega \in \Omega \\ & \forall p \in \mathbb{P} \end{aligned} \tag{9}$$

with $W(e^{i\omega})$ a weighting filter that can be utilized to specify the relative importance over the frequency range. The optimization problem (9) results in a nonconvex optimization problem in the decision variable θ. These types of problems are in general difficult to solve. By multiplication with the return difference $1 + L_p(e^{i\omega})$ a linearizing transformation is performed, resulting in a model-matching problem

$$\begin{aligned} \min_{\theta} \quad & \gamma \\ \text{s.t.} \quad & |W(e^{i\omega}) \left((1 - M(e^{i\omega}))L_p(e^{i\omega}, \theta) - M(e^{i\omega})\right)| < \gamma \\ & \forall \omega \in \Omega \\ & \forall p \in \mathbb{P} \end{aligned} \tag{10}$$

which can be viewed as a second order cone optimization problem that is convex in θ. In general, the optimization problem that is posed in (9) is not equivalent to (10). The optimization problems (10) and (9) are equivalent if there exists a $\theta^\star$ such that $T_p(e^{i\omega}, \theta^\star) = M(e^{i\omega})\ \forall p \in \mathbb{P}$. In any other case, the optimal solution $\theta^\star$ of (10) is equivalent to (9) if the weighting filter in (9) is substituted with $W(e^{i\omega})(1 + L_p(e^{i\omega}, \theta^\star))$.

3.4 Stability

In order to ensure local stability of the gyroscope for each $G_p(e^{i\omega})$, a constraint in the Nyquist diagram is introduced, similar to (Kunze et al., 2007). To this purpose, first the Nyquist theorem is presented, after which a simplified version is proposed such that stability requirement (a) is satisfied. To this end, define by $\mathcal{C}$ the closed contour that encircles the exterior of the unit disc. Furthermore, let P denote the number of unstable poles of $L_p(e^{i\omega}, \theta)$, Z the number of zeroes encircled by $\mathcal{C}$, i.e., the number of unstable closed-loop poles of $T_p(e^{i\omega}, \theta)$ and N the number of clockwise encirclements of $L_p(e^{i\omega}, \theta)$ around the the point $(-1, 0i)$.

Theorem 1. (Nyquist stability criterion). The closed-loop is stable if and only if $L_p(e^{i\omega}, \theta)$ makes $N = Z - P$ clockwise encirclements around the point $(-1, 0i)$, and $L_p(e^{i\omega}, \theta)$ does not pass through the point $(-1, 0i)$ (Skogestad and Postlethwaite, 2005).

The proof is based on Cauchy's argument principle and the reader is referred to (Skogestad and Postlethwaite, 2005) for it. A simplified case follows if the plant and the controller are stable, i.e., $P = 0$.

Corollary 1. (Simplified Nyquist theorem). Assume that $L_p(e^{i\omega}, \theta)$ has no unstable poles. Then the closed-loop system is stable if and only if $L_p(e^{i\omega}, \theta)$ does not encircle nor cross the point $(-1, 0i)$.

Proof. The proof follows from Theorem 1 by taking $Z = P = 0$. □

Since the gyroscope is stable and the controller, based on the FIR structure, is also stable, Corollary 1 represents a condition to guarantee local stability of the closed-loop system. In order to ensure that the Nyquist curve, evaluated for $\omega \geq 0$, does not cross nor encircle the critical point, it is restricted to lie below a line in the complex plane. This is graphically displayed in Figure 5 and results in the following corollary

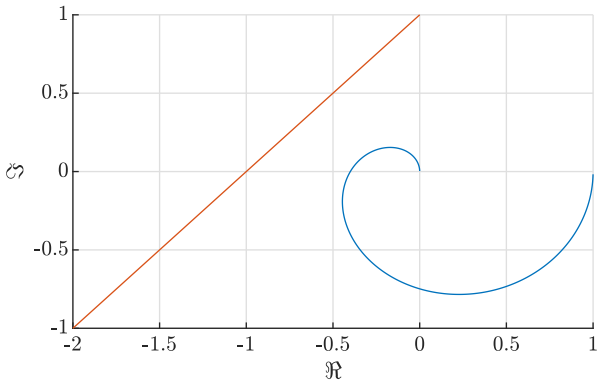

Fig. 5. Graphical interpretation of the simplified Nyquist stability criterion. The line (orange) restricts the Nyquist curve to lie to the right of the critical point $(-1, 0i)$. The Nyquist curve $L_p(e^{i\omega}, \theta)$ (blue) is shown for a constant operating condition p and fixed θ.

Corollary 2. Suppose that $L_p(e^{i\omega}, \theta)$ has no unstable poles and that the image of $L_p(e^{i\omega}, \theta)$ exists below the line

$$z = x + i\alpha(x + 1)$$

in the complex plane, with $x \in \mathbb{R}$ and $\alpha > 0 \in \mathbb{R}$. Then the closed-loop system is stable and $L_p(e^{i\omega}, \theta)$ satisfies that

$$\Im\left\{L_p(e^{i\omega}, \theta)\right\} < \alpha\left(\Re\left\{L_p(e^{i\omega}, \theta)\right\} + 1\right). \tag{11}$$

In this corollary, the Nyquist curve is constrained to lie below a line, with slope α, in the complex plane and provides a sufficient condition for local stability of the closed-loop system in Figure 3 at each operating condition p. However, global stability with respect to the controller implementation in Figure 4 can in general be guaranteed only for sufficiently slow variations of the scheduling parameters.

3.5 Fixed order LPV controller synthesis

Combining the performance conditions (10) and the stability conditions (11), which have been introduced in the previous subsections, a convex optimization problem for data-driven synthesis of fixed order LPV FIR controllers is formulated

$$\begin{aligned} \min_{\theta} \quad & \gamma \\ \text{s.t.} \quad & |W(e^{i\omega})\left((1-M(e^{i\omega}))L_p(e^{i\omega},\theta)-M(e^{i\omega})\right)| < \gamma \\ & \Im\left\{L_p(e^{i\omega},\theta)\right\} < \alpha\left(\Re\left\{L_p(e^{i\omega},\theta)\right\}+1\right) \\ & \forall \omega \in \Omega \\ & \forall p \in \mathbb{P}. \end{aligned} \tag{12}$$

The FIR structure (7) and a linear parameterization of the controller (8) result in an optimization problem (12) that is convex in the variables θ. However, the optimization problem has an infinite number of constraints. A practical approach to solve (12) is to sample the frequency space $\Omega = \{\omega^k\}_{k=1}^{N_\omega}$ and the scheduling space $\mathcal{P} = \{p^{(\tau)}\}_{\tau=1}^{N_p}$, which results in a finite-dimensional convex optimization problem that can be solved as a set of linear matrix inequalities or as a second-order cone optimization problem. Remark that sampling the scheduling and frequency spaces is also in-line with the availability of such data in practice. It is of importance that Ω expresses the relevant frequencies, such that the sampled condition (11) implies local stability (Karimi and Galdos, 2010). Additionally, $\mathcal{P}$ is chosen such that the sampled version of (6) actually implies the performance bound. Note that there exist methods that can be used to optimally determine such a set of operating points, see, e.g., (Vizer and Mercere, 2014; Sharif, 2018).

4. RESULTS

Using the proposed methodology, data-driven control design for a CMG is considered in a simulation study according to the experimental conditions given in Section 2.3. In terms of control specifications, we would like to achieve reference tracking of q_4 through actuation of τ_2, according to the control interconnection in Figure 3. Performance is characterized through specifications on the rise-time which should be less than 1 seconds and an overshoot of less than 5%. These specifications are expressed in terms of the model-matching filter $M(e^{i\omega})$. A weighting filter $W(e^{i\omega})$ is designed such that it emphasizes the bandwidth region of the model-matching filter and the resonance frequencies of the system. These filters are shown in Figure 6. It can be observed from the FRF data in Figure 2 that the system contains integral action in the low-frequency range. Remark that this this does not violate the assumptions posed on the plant. Furthermore, resonances that shift w.r.t. the operating condition are observed. To cope with this, a 2nd-order FIR controller structure is proposed. Additionally, the basis functions $\{\phi_j^\ell\}_{\ell=0,j=1}^{n_b=2,n=2}$ are chosen to have affine dependence on the operating point p, i.e., $\{\phi_j^\ell\}_{j=1}^{n} = \{1, p\}\ \forall \ell$. Note that in terms of implementation, this corresponds to the controller

$$u(kT_s) = \sum_{\ell=0}^{n_b=2} \left(c_1^\ell + c_2^\ell p(kT_s)\right) e\left((k-\ell)T_s\right), \tag{13}$$

where k denotes the discrete-time (sample index).

First an LTI FIR controller has been synthesized for the gyroscope for a nominal operating point $p = 0$, (see Figure 2) for which the controller coefficients are given in Table 2. The performance hereof is evaluated based on a step-response shown in Figure 7, from which we can observe

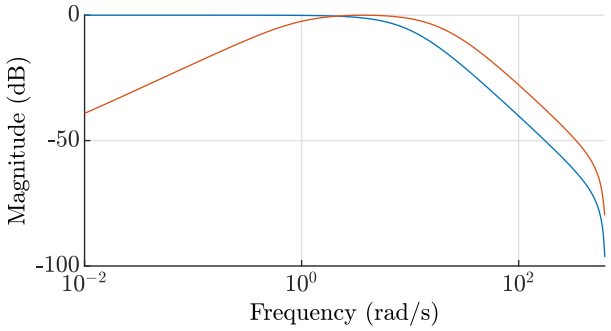

Fig. 6. Magnitude plot of the model-matching filter $M(e^{i\omega})$ in blue and the weighting filter $W(e^{i\omega})$ in orange.

that it results in a stable behavior and satisfactory performance at the operating point the controller is designed at. However, when evaluated over the entire grid of operating points, a significant loss in performance is observed and in the worst case it results in a loss of stability. Next, an LPV FIR controller has been synthesized according to the presented approach. The local step responses are shown in Figure 7 and the controller coefficients θ can be found in Table 2. The LPV controller is able to adapt the controller coefficients to the operating conditions of the gyroscope and, therefore, providing a significant increase of performance whilst maintaining local stability over the scheduling region.

Table 2. Controller coefficients $\{c_j^\ell\}_{\ell,j}^{n_b,n}$ for $n_b = 2$ and $n = 2$, for values of $p \in [-1\ 1]$. LPV (top) and LTI controller parameters (bottom) respectively. The LTI controller parameters are shown for $p = \{-1, 0, 1\}$.

$j \backslash \ell$	0	1	2
1	-186.6286	371.9496	-186.5282
2	37.5585	-75.7015	37.4940
$p=-1$	-257.3616	513.8426	-257.2289
$p=0$	-171.7561	342.3943	-171.7591
$p=1$	-128.8593	256.3311	-128.9662

A reference tracking simulation has been conducted to assess the tracking performance of the synthesized LPV FIR controller on the gyroscope (1). Here the objective is to track a smooth reference trajectory for a time-varying scheduling signal p. The controller is implemented according to Figure 4, where in this case, in (13) p is time-varying, i.e., $p(kT_s) = \dot{q}_{1,*}(kT_s)$ measured online. Since the LPV controller design is based on local linear models around a moving operating point, stability and performance theoretically can only be guaranteed in a neighborhood of the considered operating points of the closed-loop system. However, it can be observed from Figure 8 that stability and satisfactory performance are achieved over a large operating range of the scheduling variable (and inherently the angles and velocities of the bodies comprising the gyroscope).

5. CONCLUSION

In this paper, it is demonstrated how to synthesize a fixed order LPV FIR controller directly from local frequency

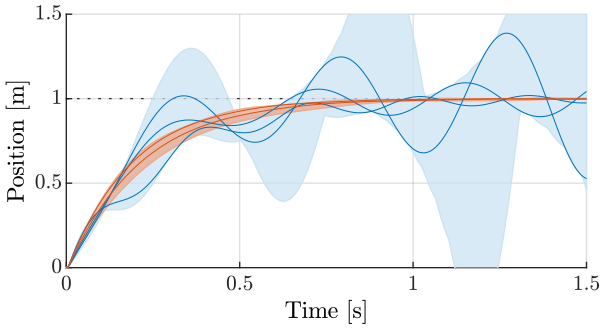

Fig. 7. Unit step response of the closed-loop system evaluated at randomly selected frozen operating points $\{p^{(\tau)}\} \in \mathbb{P}$, using the 2nd order LTI and LPV FIR controllers in blue and orange lines, respectively. The LTI controller that is used is equal to the one for $p = 0$ given in Table 2. The blue and orange shaded areas indicate the regions that cover all trajectories for frozen $\{p^{(\tau)}\} \in \mathbb{P}$ for the LTI and LPV controllers, respectively.

domain measurement data of a CMG. It is shown how to incorporate control specifications during control design, such that reference tracking of a CMG for a wide operating range is achieved. The performance of this controller is evaluated on a simulation example, indicating that indeed reference tracking for a wide operating range is achieved.

REFERENCES

Abbas, H.S., Ali, A., Hashemi, S.M., and Werner, H. (2014). LPV state-feedback control of a control moment gyroscope. *Control Engineering Practice*, 24, 129–137.

Bedrossian, N.S., Bhatt, S., Kang, W., and Ross, I.M. (2009). Zero-propellant maneuver guidance. *IEEE Control Systems Magazine*, 29(5), 53–73.

Bloemers, T. and Tóth, R. (2019). Equations of Motion of a Control Moment Gyroscope. Technical report, Eindhoven University of Technology.

Formentin, S., Piga, D., Tóth, R., and Savaresi, S.M. (2016). Direct learning of LPV controllers from data. *Automatica*, 65, 98–110.

Karimi, A. and Emedi, Z. (2013). $\mathcal{H}_\infty$ gain-scheduled controller design for rejection of time-varying narrow-band disturbances applied to a benchmark problem. *European Journal of Control*, 19(4), 279–288.

Karimi, A. and Galdos, G. (2010). Fixed-order $\mathcal{H}_\infty$ controller design for nonparametric models by convex optimization. *Automatica*, 46(8), 1388–1394.

Koelewijn, P., Cisneros, P., Werner, H., and Tóth, R. (2018). LPV Control of a Gyroscope with Inverted Pendulum Attachment. In *Proc. of the 2nd IFAC Workshop on Linear Parameter Varying Systems*. Florianopolis, Brazil.

Kristiansen, R., Egeland, O., and Nicklasson, P.J. (2005). A comparative study of actuator configurations for satellite attitude control. *Modeling, Identification and Control*, 25(4), 201–220.

Kunze, M., Karimi, A., and Longchamp, R. (2007). Gain-scheduled controller design by linear programming. In *Proc. of the European Control Conference*, 5432–5438. Kos, Greece.

Liceaga, J., Liceaga, E., and Amézquita, L. (2005). Multivariable gyroscope control by individual channel design. In *Proc. of the IEEE Conference on Control Applications*, 785–790. Toronto, Canada.

Maciejowski, J.M. (1989). *Multivariable feedback design. Electronic systems engineering series*. Addison-Wesley.

Perez, T. and Steinmann, P. (2009). Analysis of ship roll gyrostabiliser control. In *Proc. of the 8th Conference on Manoeuvring and Control of Marine Craft*, 310–315. Guaruj a, Brazil.

Reyhanoglu, M. and van de Loo, J. (2006). State feedback tracking of a nonholonomic control moment gyroscope. In *Proc. of the IEEE Conference on Decision and Control*, 6156–6161. San Diego, USA.

Sharif, B. (2018). Linear Parameter Varying Control of Nonlinear Systems. *MSc thesis, Eindhoven University of Technology*.

Skogestad, S. and Postlethwaite, I. (2005). *Multivariable feedback control: analysis and design*. Wiley New York.

Theis, J., Radisch, C., and Werner, H. (2014). Self-scheduled control of a gyroscope. In *Proc. of the 19th IFAC World Congress*, 6129–6134. Cape Town, South Africa.

Vizer, D. and Mercere, G. (2014). $\mathcal{H}_\infty$-based LPV model identification from local experiments with a gap metric-based operating point selection. In *Proc. of the European Control Conference*, 388–393. Strasbourg, France.

Wassink, M.G., van de Wal, M., Scherer, C., and Bosgra, O. (2005). LPV control for a wafer stage: beyond the theoretical solution. *Control Engineering Practice*, 13(2), 231–245.

Wie, B. (2008). *Space vehicle dynamics and control*. American Institute of Aeronautics and Astronautics.

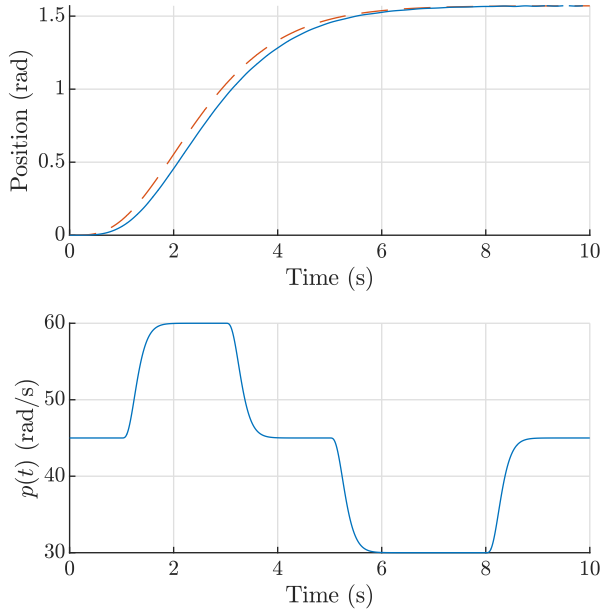

Fig. 8. Reference tracking of the gyroscope using the 2nd order LPV FIR controller. Angular position of gimbal A in blue and the reference in dashed orange (upper plot). Scheduling variable $p(kT_s) = \dot{q}_{1,*}(kT_s)$ (bottom plot).